Nanoscale

Enhanced Photocurrent Response Speed in Charge-Density-Wave Phase of TiSe2-Metal Junctions

Journal:	*Nanoscale*
Manuscript ID	NR-ART-03-2021-001810.R1
Article Type:	Paper
Date Submitted by the Author:	25-May-2021
Complete List of Authors:	Walmsley, Thayer; Vanderbilt University, Electrical Engineering and Computer Science Xu, Yaqiong; Vanderbilt University, Electrical Engineering and Computer Science

Enhanced Photocurrent Response Speed in Charge-Density-Wave Phase of $TiSe_2$-Metal Junctions

Thayer S. Walmsley[1] and Ya-Qiong Xu[,1,2]*

[1]Department of Physics and Astronomy, Vanderbilt University, Nashville, TN 37235, USA

[2]Department of Electrical Engineering and Computer Science, Vanderbilt University, Nashville, TN 37235, USA

*Correspondence to: yaqiong.xu@vanderbilt.edu

Abstract

Group IVB transition metal dichalcogenides (TMDCs) have attracted significant attention due to their predicted high charge carrier mobility, large sheet current density, and enhanced thermoelectric power. Here, we investigate the electrical and optoelectronic properties of few-layer titanium diselenide ($TiSe_2$)-metal junctions through spatial-, wavelength-, temperature-, power- and temporal-dependent scanning photocurrent measurements. Strong photocurrent responses have been detected at $TiSe_2$-metal junctions, which is likely attributed to both photovoltaic and photothermoelectric effects. A fast response time of 31 μs has been achieved, which is two orders of magnitude better than $HfSe_2$ based devices. More importantly, our experimental results reveal a significant enhancement in the response speed upon cooling to the charge-density-wave (CDW) phase transition temperature (T_{CDW} = 206 K), which may result from dramatic reduction in carrier scattering that occurs as a result of the switching between the normal and CDW phases of $TiSe_2$. Additionally, the photoresponsivity at 145 K is up to an order of magnitude higher than that obtained at room temperature. These fundamental studies not only offer insight for the photocurrent generation mechanisms of group IVB TMDC materials, but also provide a way to engineering future temperature-dependent, two-dimensional, fast electronic and optoelectronic devices.

Keywords: $TiSe_2$, photocurrent, responsivity and time, TMDC, CDW

Introduction

A new dimension of materials research was opened up with the successful isolation and characterization of graphene.[1] Its variety of excellent mechanical, electrical, and optical properties as well as its semimetallic nature have fueled many different applications and served as a platform to investigate nanoscale science. This has propelled the search for other similar two-dimensional (2D) materials. A class of materials known as transition metal dichaclogenides (TMDCs) has garnered intense interest for their superior electronic[2, 3] and optoelectronic properties.[4, 5] Though these materials are characterized by the X-M-X structure where the X represents a chalcogenide (S, Se, Te) and M represents a transition metal from groups IVB through VIIIB, the group VIB TMDCs (e.g. MoS_2) have received the most attention. Looking deeper into this class of materials one finds that group IVB TMDCs (M= Ti, Zr, Hf and X= S, Se, Te) have received relatively little attention in their single- or few-layer form even though they possess unique optical, electrical, optoelectronic, and thermoelectric properties.[6] Strong light absorption properties in the visible to the infrared region as well as enhanced thermoelectric performance with high power factors have been show in TiS_2.[7, 8] An exceptionally high charge carrier mobility of ~2,000 $cm^2V^{-1}s^{-1}$ as well as a sheet current density up to 8000 $\mu A\ \mu m^{-1}$, much higher than those of MoS_2, have been predicted for $ZrSe_2$.[9, 10] And the semiconducting $HfSe_2$ has a high predicted mobility of ~3,579 $cm^2V^{-1}s^{-}1$.[10] Furthermore, phototransistors fabricated out of $HfSe_2$ have shown strong responsivity in the visible to ultraviolet regimes in the range of hundreds of amperes per watts but with a slow response time on the order of milliseconds and only achieved under large gate voltages.[11] In addition to these materials, the nearby group VB semimetallic and semiconducting charge-density-wave (CDW) materials of

$TaSe_2$ and TaS_2 have recently demonstrated extremely fast, ultra-broadband response and ultra-high responsivity.[12, 13] All these fundamental studies hold promise for the further exploration of the optoelectronic properties of group IVB materials, such as $TiSe_2$. Many investigations have examined the optical and electrical properties of few-layer $TiSe_2$, showing a relatively high CDW phase transition temperature, T_{CDW}, of ~200 K as well as the ability to precisely control this transition temperature using an electric field.[14-18] But, previous work on optoelectronic properties of $TiSe_2$ have been focused on either angle-resolved photoemission spectroscopy measurements that reveal detailed understandings of the CDW phase transition and associated band structure[19-22] or other work that explores the observation of spontaneous gyrotropic electronic order.[23] This encourages but leaves open the exploration of few-layer $TiSe_2$ optoelectronic devices.

Here we fabricate few-layer $TiSe_2$-metal junctions using a metal transfer technique and subsequently explore their electrical and optoelectronic properties via scanning photocurrent microscopy. Strong photocurrent responses have been observed at the $TiSe_2$-metal junctions under 650 nm and 1064 nm illumination, respectively. Further studies have revealed that both the photovoltaic effect (PVE) and the photothermoelectric effect (PTE) contribute to the photocurrent generation. At 145 K, the photoresponsivities are 4.8 mA/W and 1.4 mA/W for 650 nm and 1064 nm illumination, respectively. Moreover, temporally resolved scanning photocurrent measurements demonstrate that rise and decay time constants are 31 μs and 32 μs, respectively, which are two orders of magnitude better than $HfSe_2$ based devices.[11] More importantly, we have found that the response times are two times slower when the temperature increases to 225 K. Additionally, there is up to an order of magnitude of reduction for the photocurrent responsivity at room temperature. The

significant temperature-induced changes are likely attributed to dramatic reduction in carrier scattering that occurs when $TiSe_2$ is changed from the normal to CDW phases at T_{CDW} (~ 206 K). These results signify the depth and breadth of knowledge gained from continually exploring and assessing 2D materials for optoelectronic devices and advance the understanding of group IVB TMDCs. Furthermore, this work sheds light on the critical aspects of 2D material-metal junctions for engineering future temperature-dependent fast optoelectronic devices.

Results and Discussion

A schematic of a typical $TiSe_2$ device used in the experiments is presented in Figure 1a. High quality $TiSe_2$ flakes were mechanically exfoliated from a bulk crystal onto degenerately doped SiO_2/Si substrates using the standard scotch tape method.[1] Sample thicknesses were characterized using a Bruker Dimension Icon Atomic Force Microscope, ranging from ~20 nm to ~49 nm. Au electrodes pre-patterned on a sacrificial silicon substrate were then transferred onto $TiSe_2$ flakes to nearly eliminate the Fermi-level pinning effect that has plagued many other TMDC material based devices.[24] The inset of Figure 1c shows a $TiSe_2$ device with a thickness of ~31 nm.

Raman spectroscopy has been used to identify the quality of $TiSe_2$ flakes. As shown in Figure 1b two dominant peaks are located at ~134 cm^{-1} and ~197 cm^{-1}, respectively, corresponding to the in plane (E_g) and out of plane (A_{1g}) vibrational modes of the Se atoms in $TiSe_2$, respectively.[15-17] No significant difference was noted in these peaks based on our sample thicknesses. A weak peak is also seen at ~305 cm^{-1}, likely resulting from acoustic phonons in the underlying silicon substrate and potentially the combination of the two different dominant modes.[15, 25, 26] Moreover, the absence of additional peaks indicates the

pristine nature of the sample as it is common for peaks to arise during the oxidation process associated with trigonal (~253 cm^{-1}) and amorphous (~233 cm^{-1}) selenium that replace the dominance of the aforementioned active Raman modes.[27-29] Temperature-dependent electrical resistance measurements were further performed to characterize and assess device performance. A broad resistance peak centered at ~180 K is observed (black in Figure 1c), consistent with previous electrical transport investigations of $TiSe_2$.[14, 18, 27, 30] This anomalous resistivity peak is attributed to a crossover between a low temperature regime where electron-like carriers dominate the conductivity to a high temperature regime where thermally activated hole-like carriers dominate.[31] Additionally, a ratio for R_{max}/R_{300} of ~1.3 is observed that is comparable to molecular-beam epitaxy grown $TiSe_2$ thin films,[30] indicating the high quality of the mechanically exfoliated $TiSe_2$ flakes. To determine the CDW phase transition temperature (T_{CDW}) in $TiSe_2$, the derivative with respect to temperature of the resistance-temperature graph is calculated (red in Figure 1c) and the local minimum is found as ~206 K (T_{CDW}), which is consistent with previous reports.[14, 18, 27, 30] To explore optoelectronic properties of $TiSe_2$, spatially resolved scanning photocurrent measurements were performed in an Olympus microscopy setup.[32] A continuous wave laser beam (NKT Photonics SuperK Supercontinuum Laser) was expanded and then focused by a 40X Olympus objective (N.A. = 0.6) into a diffraction-limited spot (~ 1 μm). After that, the laser spot was scanned over the device using nanometer-scale spatial resolution piezo-controlled mirrors. As shown in Figures 2a and S1a, remarkable photocurrent responses were observed under 1064 nm and 650 nm illumination, respectively. The corresponding reflection images (Figures 2b and S1b) that were recorded simultaneously could be used to locate the positions of photocurrent signals. The electrodes

are outlined in gray dashed lines, with D and S representing the drain and source contacts, respectively. The $TiSe_2$ flakes are outlined in purple. Strong photocurrent signals ($I_{pc} = I_{laser} - I_{dark}$) are observed at the $TiSe_2$-metal junctions, likely due to the Fermi level alignment at the junctions which leads to built-in electric fields that can efficiently separate photo-excited electron-hole pairs (EHPs) to generate photocurrent signals. This suggests that the PVE plays an important role in the photocurrent generation at $TiSe_2$-metal junctions.[33] When the laser scans across the drain (source) contact, photo-excited EHPs are separated, generating a negative (positive) photocurrent due to the larger work function of the $TiSe_2$ flake relative to gold contacts that produces downward band bending.[34] To further clarify the photocurrent generation mechanisms present in the $TiSe_2$-metal junction, line profiles of photocurrent intensity under 1064 nm illumination are extracted across the junctions at 145 K and 280 K (Figures 2c and 2d), respectively, where the photocurrent intensities were normalized for clarity. By comparing the photocurrent profiles with the Gaussian fittings (solid red curves), we notice a strong photocurrent "tail" in the gold electrode region for the environmental temperature below the T_{CDW} as indicated by the blue arrows, suggesting that the PTE also contributes to the photocurrent generation at the junction for $TiSe_2$ in CDW phase.[35, 36] This is consistent with previous reports that $TiSe_2$ possesses a high thermoelectric power below $T_{CDW,}$[37-39] inducing heat gradients at the $TiSe_2$-metal junction and thus giving rise to a thermoelectric current.[40] Similar results are found under 650 nm illumination (Figure S1).

The photoresponse dynamics were also examined through temporally resolved scanning photocurrent measurements for both above and below T_{CDW}. In these experiments, the addition of an optical chopper to the light path allowed for the application of ON/OFF

light modulation while photocurrent signals were recorded as a function of time. The limit of the measurement circuit is around 8 μs.[41, 42] Two cycles of a typical temporal response under 1064 nm illumination at 145 K for the $TiSe_2$ device is shown in Figure 3a. The device maintained consistency in its optoelectronic performance over thousands of cycles demonstrating its reliability. Using a single exponential function to fit the rise and decay portions of the time response curve, rise and decay time constants are found for both above and below the CDW phase transition temperatures (Figure 3b). The photoresponse times are significantly reduced upon cooling to T_{CDW}. To further examine this difference snapshots of the rise and decay curves are shown in Figure 3c and 3d, respectively. At 225 K (above T_{CDW}), rise and decay time constants are 60 μs and 66 μs, respectively. Moreover, we have found that rise and decay time constants of 31 μs and 32 μs are achieved at 145 K (below T_{CDW}), which are as twice fast as those above T_{CDW}, two orders of magnitude better than $HfSe_2$ based devices.[11] The greatly improved response times below the CDW phase transition temperature is likely attributed to dramatic reduction in carrier scattering that occurs as a result of the switching between the normal and CDW phases of $TiSe_2$.[43] It is well-known that two important factors that limit the response time of a device are RC time constant and carrier transit time.[44] For $TiSe_2$ in CDW phase, the reduction in carrier scattering results in short carrier transit time, leading to fast photocurrent response. To determine the exact nature of these interactions further focus on the photodynamic response of $TiSe_2$ is warranted.

Next we explore how the CDW phase transition influences the responsivity of $TiSe_2$-metal junctions under laser illumination (Figure 4a). Here, the laser beam with a diffraction limit about 1 μm has been locally focused at the $TiSe_2$-metal interfaces, which

is different from some studies that the beam sizes are larger than the devices.[12, 45, 46] Positive and negative photocurrent signals are found at source and drain regions, respectively, in which the positive response has been used to analyze the responsivity in Figure 4a. Our experimental results reveal a significant enhancement in the responsivity of the devices under cooling and a doubling of the rate of photocurrent increase below T_{CDW}. Maximum responsivities at 145 K have been achieved to be 4.8 mA/W under 650 nm illumination and 1.4 mA/W under 1064 nm illumination, respectively, up to an order of magnitude higher than those obtained at room temperature. The relatively small responsivity of $TiSe_2$ under 1064 nm illumination is likely attributed to the lower optical absorption for 1064 nm excitation than that for 650 nm excitation.[47] This further suggests that in the CDW phase, the carrier scattering reduction leads to short carrier transit time,[43, 48] improving the collection of photoexcited EHPs and thus enhancing the photocurrent generation efficiency. Moreover, linear power-dependent relationships were observed for both 650 nm and 1064 nm illumination at 145 K (Figure 4b). This linear trend is expected as the increased number of incident photons from a higher power results in an increased generation of EHPs.

Conclusion

We systematically investigate electrical and optoelectronic properties of few-layer $TiSe_2$-metal junctions. Remarkable photocurrent responses have been detected at the $TiSe_2$-metal junctions, likely resulting from both the PVE and the PTE. A fast response time approaching to 31 μs has been achieved, which are two orders of magnitude better than $HfSe_2$ based devices. More importantly, we have found that the photocurrent responsivity and speed increase significantly upon the temperature cooling to T_{CDW}, which is likely

attributed to dramatic reduction in carrier scattering that occurs as a result of the switching from the normal to CDW phases in $TiSe_2$. Not only do these results further the understanding of group IVB TMDC materials but also offer promise for future investigations into these enticing class of materials, opening new avenues for future 2D optoelectronic engineering.

Methods

Bulk $TiSe_2$ crystals from *2D Semiconductors* were used to prepare the devices. These bulk crystals were mechanically exfoliated using the scotch tape method onto degenerately *p*-doped silicon substrates with 290 nm of thermally grown SiO_2.[1] After identifying thin flakes as targets for devices, an electrode transfer procedure was performed.[24, 49] First, 50 nm thick gold electrode patterns were created using standard photolithography and electron beam deposition procedures. The sacrificial substrate was then diced to facilitate manageable sized pattern transfers. The gold electrodes on the sacrificial substrate were then treated with hexamethyldisilazane (HMDS) for 20 minutes in a 180 °C sealed chamber. Two layers of 495 A11 polymethyl methacrylate (PMMA) were spin coated at 2500 RPM with an intermediate hard bake step. A polydimethylsiloxane (PDMS) stamp on a glass slide was then used to pick up the PMMA with the gold electrode pattern off of the sacrificial substrate. Using a home-built precision transfer stage, the gold electrodes were able to be aligned with the target flake. After that, the PDMS could be released from the fabricated device by heating the substrate and subsequently raising the stamp. Devices were then mounted on chip carriers to facilitate electrical and optoelectronic characterization in a Janis ST-500 microscopy cryostat under high vacuum ($\approx 10^{-6}$ Torr).[50]

Author contributions

Y. X. and T. S.W. conceived of the research idea. T.S.W fabricated devices, performed the experiments, and analyzed the data. All authors contributed to the final version of the manuscript. Y. X. supervised the project.

Conflicts of interest

The authors declare no competing financial interests.

Acknowledgements

This work was supported by the National Science Foundation (ECCS-1810088 and CBET-1805924).

Figures

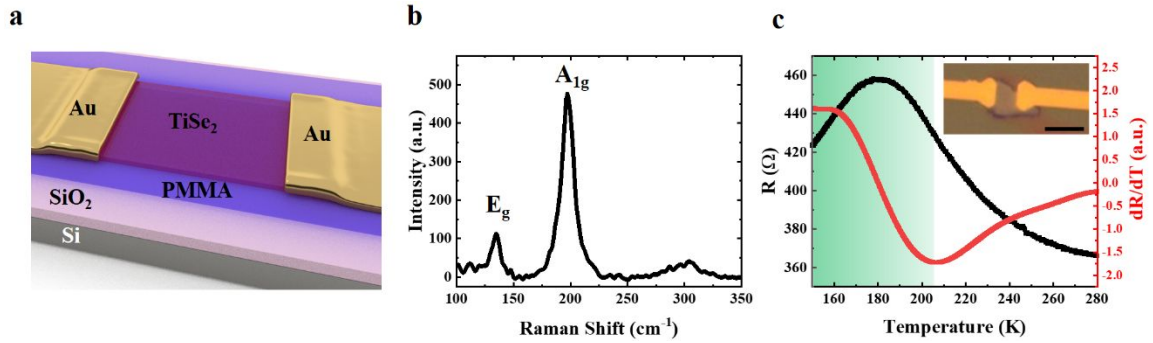

Figure 1. (a) A schematic illustrating the layout of a $TiSe_2$ device. (b) Raman spectrum of a typical few-layer $TiSe_2$ flake at room temperature. Two strong peaks are seen at ~134 cm^{-1} and ~197 cm^{-1}, respectively, which match well with the E_g and A_{1g} optical phonon modes of 1T-$TiSe_2$. An additional weak peak is observed at ~305 cm^{-1}, which may result from the overlap of the two phonon processes of $TiSe_2$ and a remnant of the silicon substrate. (c) Temperature-dependent resistance measurements show the characteristic resistivity peak (black). A broad maximum is noted at ~180K. A ratio for R_{max}/R_{300} of ~1.3 is observed, indicating the high quality of the mechanically exfoliated $TiSe_2$. The first derivative of the temperature-dependent resistance with respect to temperature is shown in red. The minimum of this curve, ~206 K, corresponds to the CDW phase transition temperature. The green background represents the CDW phase. Inset in (c) is an optical micrograph of a $TiSe_2$ device. The scale bar is 10 μm.

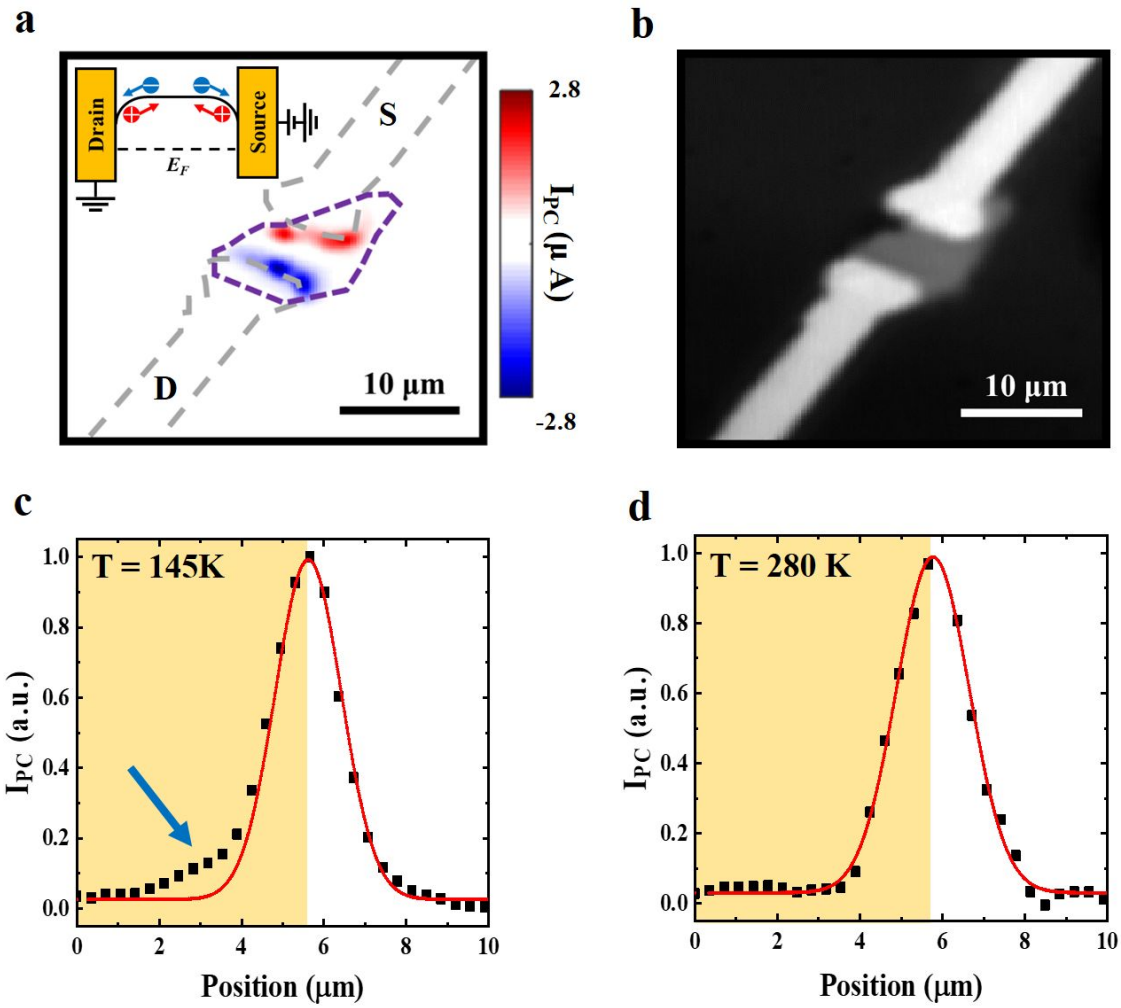

Figure 2. (a) Spatially resolved photocurrent and (b) reflection images of the device at 145 K show strong photocurrent responses at $TiSe_2$-metal junctions. The power of the 1064 nm laser is ~1.86 mW. The inset of (a) shows a circuit diagram of the $TiSe_2$ device depicting the current direction for the respective laser scanning locations. The laser scan across the drain (source) contact, resulting in the observed negative (positive) photocurrent signals. Photocurrent responses across the $TiSe_2$-metal junctions at (c) 145 K and (d) 280 K, respectively. The black dots and red solid curves are experimental data and the related Gaussian fittings, respectively. The photocurrent "tail" on the electrode is highlighted by the blue arrow. The yellow backgrounds represent the positions of the electrodes.

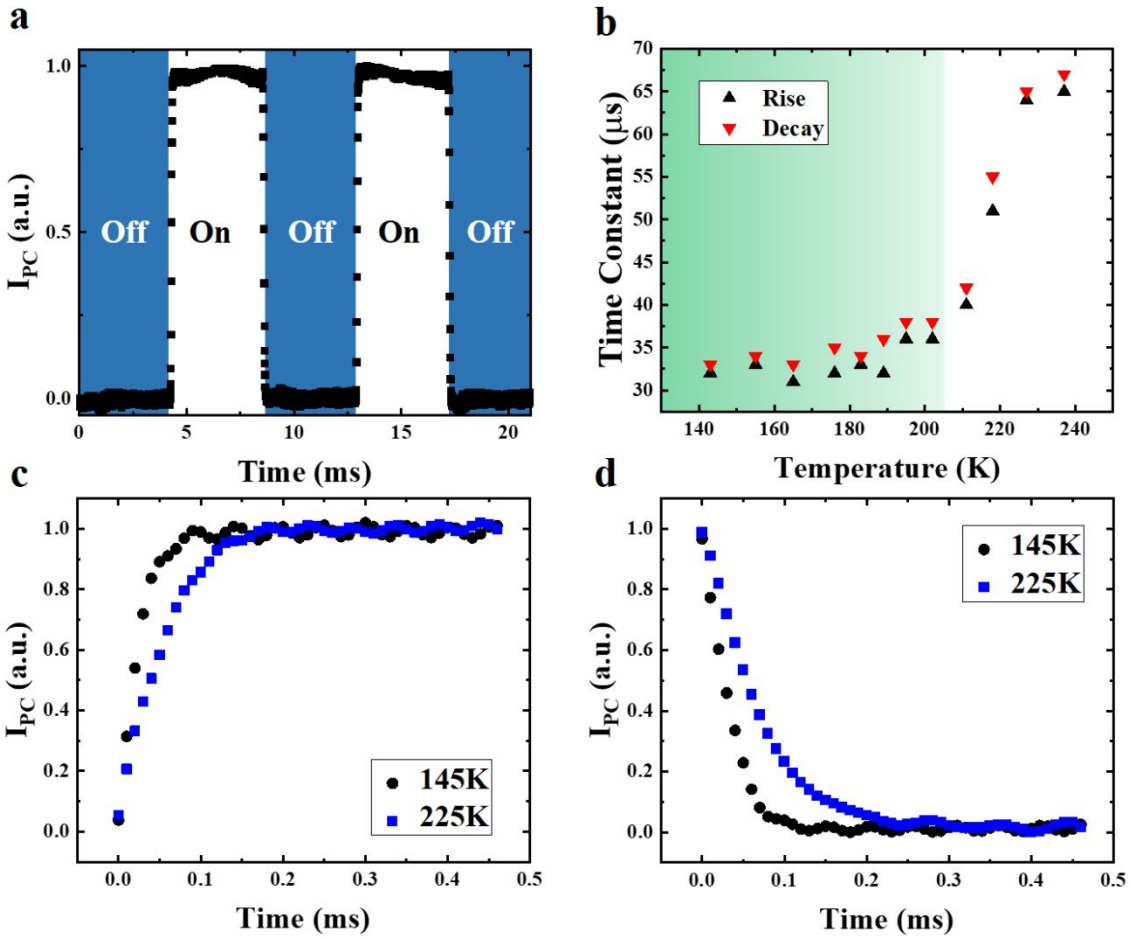

Figure 3. (a) Typical temporal response of the device at 145 K under 1064 nm illumination. (b) Temperature-dependent response for the rise and decay time constants as shown in black and red triangles, respectively. The green background represents the CDW phase. To further elucidate this change, snapshots of the rise (c) and decay (d) time curves are shown, respectively.

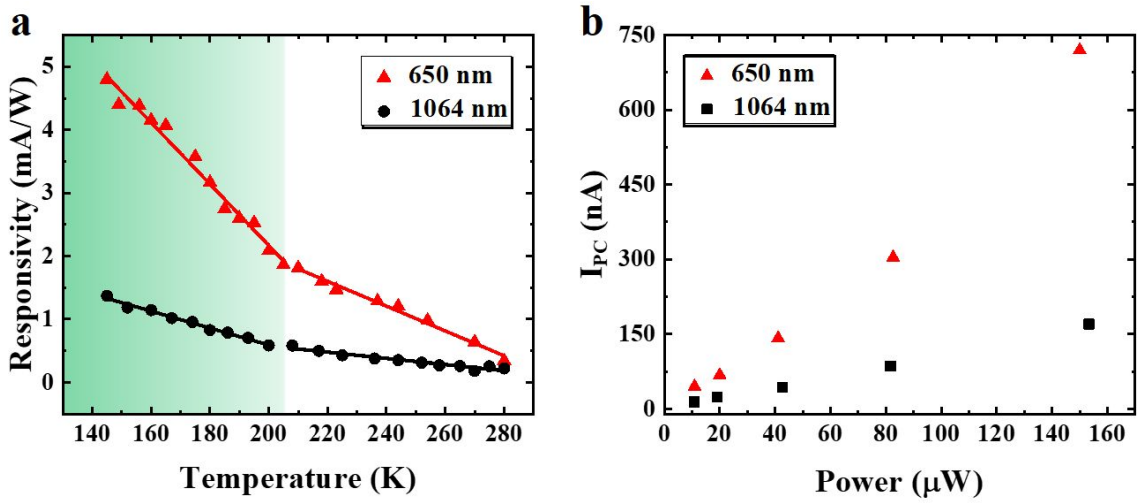

Figure 4. (a) Temperature-dependent photocurrent measurements reveal a significant increase in the responsivity of the device with decreasing temperature. The rate in which the photocurrent changes approximately doubles below T_{CDW} as indicated by the fitted slopes. The green background represents the CDW phase. (b) Power-dependent photocurrent measurements under 650 nm (red) and 1064 nm (black) illumination at 145 K show linear relationships with power.

References:

1. Novoselov, K. S.; Geim, A. K.; Morozov, S. V.; Jiang, D.; Zhang, Y.; Dubonos, S. V.; Grigorieva, I. V.; Firsov, A. A., Electric Field Effect in Atomically Thin Carbon Films. *Science* **2004,** *306* (5696), 666-669.
2. Das, S.; Chen, H.-Y.; Penumatcha, A. V.; Appenzeller, J., High Performance Multilayer MoS_2 Transistors with Scandium Contacts. *Nano Letters* **2013,** *13* (1), 100-105.
3. Wang, H.; Yu, L.; Lee, Y.-H.; Shi, Y.; Hsu, A.; Chin, M. L.; Li, L.-J.; Dubey, M.; Kong, J.; Palacios, T., Integrated Circuits Based on Bilayer MoS_2 Transistors. *Nano Letters* **2012,** *12* (9), 4674-4680.
4. Lopez-Sanchez, O.; Lembke, D.; Kayci, M.; Radenovic, A.; Kis, A., Ultrasensitive photodetectors based on monolayer MoS_2. *Nature Nanotechnology* **2013,** *8*, 497.
5. Yin, Z.; Li, H.; Li, H.; Jiang, L.; Shi, Y.; Sun, Y.; Lu, G.; Zhang, Q.; Chen, X.; Zhang, H., Single-Layer MoS_2 Phototransistors. *ACS Nano* **2012,** *6* (1), 74-80.
6. Yan, C.; Gong, C.; Wangyang, P.; Chu, J.; Hu, K.; Li, C.; Wang, X.; Du, X.; Zhai, T.; Li, Y.; Xiong, J., 2D Group IVB Transition Metal Dichalcogenides. *Advanced Functional Materials* **2018,** *28* (39), 1803305.
7. Wan, C.; Gu, X.; Dang, F.; Itoh, T.; Wang, Y.; Sasaki, H.; Kondo, M.; Koga, K.; Yabuki, K.; Snyder, G. J.; Yang, R.; Koumoto, K., Flexible n-type thermoelectric materials by organic intercalation of layered transition metal dichalcogenide TiS_2. *Nature Materials* **2015,** *14* (6), 622-627.
8. Ge, Y.; Zhu, Z.; Xu, Y.; Chen, Y.; Chen, S.; Liang, Z.; Song, Y.; Zou, Y.; Zeng, H.; Xu, S.; Zhang, H.; Fan, D., Broadband Nonlinear Photoresponse of 2D TiS_2 for Ultrashort Pulse Generation and All-Optical Thresholding Devices. *Advanced Optical Materials* **2018,** *6* (4), 1701166.
9. Fiori, G.; Bonaccorso, F.; Iannaccone, G.; Palacios, T.; Neumaier, D.; Seabaugh, A.; Banerjee, S. K.; Colombo, L., Electronics based on two-dimensional materials. *Nature Nanotechnology* **2014,** *9* (10), 768-779.
10. Zhang, W.; Huang, Z.; Zhang, W.; Li, Y., Two-dimensional semiconductors with possible high room temperature mobility. *Nano Research* **2014,** *7* (12), 1731-1737.
11. Yin, L.; Xu, K.; Wen, Y.; Wang, Z.; Huang, Y.; Wang, F.; Shifa, T. A.; Cheng, R.; Ma, H.; He, J., Ultrafast and ultrasensitive phototransistors based on few-layered $HfSe_2$. *Applied Physics Letters* **2016,** *109* (21), 213105.
12. Wang, L.; Wang, J.; Liu, C.; Xu, H.; Li, A.; Wei, D.; Liu, Y.; Chen, G.; Chen, X.; Lu, W., Distinctive Performance of Terahertz Photodetection Driven by Charge-Density-Wave Order in CVD-Grown Tantalum Diselenide. *Advanced Functional Materials* **2019,** *29* (45), 1905057.
13. Wu, D.; Ma, Y.; Niu, Y.; Liu, Q.; Dong, T.; Zhang, S.; Niu, J.; Zhou, H.; Wei, J.; Wang, Y.; Zhao, Z.; Wang, N., Ultrabroadband photosensitivity from visible to terahertz at room temperature. *Science Advances* **2018,** *4* (8), eaao3057.
14. Di Salvo, F. J.; Moncton, D. E.; Waszczak, J. V., Electronic properties and superlattice formation in the semimetal $TiSe_2$. *Physical Review B* **1976,** *14* (10), 4321-4328.
15. Holy, J. A.; Woo, K. C.; Klein, M. V.; Brown, F. C., Raman and infrared studies of superlattice formation in $TiSe_2$. *Physical Review B* **1977,** *16* (8), 3628-3637.

16. Snow, C. S.; Karpus, J. F.; Cooper, S. L.; Kidd, T. E.; Chiang, T. C., Quantum Melting of the Charge-Density-Wave State in 1T-$TiSe_2$. *Physical Review Letters* **2003,** *91* (13), 136402.
17. Wang, H.; Chen, Y.; Duchamp, M.; Zeng, Q.; Wang, X.; Tsang, S. H.; Li, H.; Jing, L.; Yu, T.; Teo, E. H. T.; Liu, Z., Large-Area Atomic Layers of the Charge-Density-Wave Conductor $TiSe_2$. *Advanced Materials* **2018,** *30* (8), 1704382.
18. Li, L. J.; O'Farrell, E. C. T.; Loh, K. P.; Eda, G.; Özyilmaz, B.; Castro Neto, A. H., Controlling many-body states by the electric-field effect in a two-dimensional material. *Nature* **2016,** *529* (7585), 185-189.
19. Chen, P.; Chan, Y. H.; Fang, X. Y.; Zhang, Y.; Chou, M. Y.; Mo, S. K.; Hussain, Z.; Fedorov, A. V.; Chiang, T. C., Charge density wave transition in single-layer titanium diselenide. *Nature Communications* **2015,** *6* (1), 8943.
20. Sugawara, K.; Nakata, Y.; Shimizu, R.; Han, P.; Hitosugi, T.; Sato, T.; Takahashi, T., Unconventional Charge-Density-Wave Transition in Monolayer 1T-$TiSe_2$. *ACS Nano* **2016,** *10* (1), 1341-1345.
21. Chen, P.; Chan, Y. H.; Fang, X. Y.; Mo, S. K.; Hussain, Z.; Fedorov, A. V.; Chou, M. Y.; Chiang, T. C., Hidden Order and Dimensional Crossover of the Charge Density Waves in $TiSe_2$. *Scientific Reports* **2016,** *6* (1), 37910.
22. Chen, P.; Chan, Y. H.; Wong, M. H.; Fang, X. Y.; Chou, M. Y.; Mo, S. K.; Hussain, Z.; Fedorov, A. V.; Chiang, T. C., Dimensional Effects on the Charge Density Waves in Ultrathin Films of $TiSe_2$. *Nano Letters* **2016,** *16* (10), 6331-6336.
23. Xu, S.-Y.; Ma, Q.; Gao, Y.; Kogar, A.; Zong, A.; Mier Valdivia, A. M.; Dinh, T. H.; Huang, S.-M.; Singh, B.; Hsu, C.-H.; Chang, T.-R.; Ruff, J. P. C.; Watanabe, K.; Taniguchi, T.; Lin, H.; Karapetrov, G.; Xiao, D.; Jarillo-Herrero, P.; Gedik, N., Spontaneous gyrotropic electronic order in a transition-metal dichalcogenide. *Nature* **2020,** *578* (7796), 545-549.
24. Liu, Y.; Guo, J.; Zhu, E.; Liao, L.; Lee, S.-J.; Ding, M.; Shakir, I.; Gambin, V.; Huang, Y.; Duan, X., Approaching the Schottky–Mott limit in van der Waals metal–semiconductor junctions. *Nature* **2018,** *557* (7707), 696-700.
25. Uchida, S.; Sugai, S., Infrared and Raman studies on commensurate CDW states in transition metal dichalcogenides. *Physica B+C* **1981,** *105* (1), 393-399.
26. Temple, P. A.; Hathaway, C. E., Multiphonon Raman Spectrum of Silicon. *Physical Review B* **1973,** *7* (8), 3685-3697.
27. Sun, L.; Chen, C.; Zhang, Q.; Sohrt, C.; Zhao, T.; Xu, G.; Wang, J.; Wang, D.; Rossnagel, K.; Gu, L.; Tao, C.; Jiao, L., Suppression of the Charge Density Wave State in Two-Dimensional 1T-$TiSe_2$ by Atmospheric Oxidation. *Angewandte Chemie International Edition* **2017,** *56* (31), 8981-8985.
28. Li, I. L.; Ruan, S. C.; Li, Z. M.; Zhai, J. P.; Tang, Z. K., Resonant Raman study of confined Se single helix and Se8 rings. *Applied Physics Letters* **2005,** *87* (7), 071902.
29. Poborchii, V. V.; Kolobov, A. V.; Caro, J.; Zhuravlev, V. V.; Tanaka, K., Dynamics of Single Selenium Chains Confined in One-Dimensional Nanochannels of $AlPO_4$-5: Temperature Dependencies of the First- and Second-Order Raman Spectra. *Physical Review Letters* **1999,** *82* (9), 1955-1958.
30. Wang, Y.; Nakano, M.; Kashiwabara, Y.; Matsuoka, H.; Iwasa, Y., Transport properties of a few nanometer-thick $TiSe_2$ films grown by molecular-beam epitaxy. *Applied Physics Letters* **2018,** *113* (7), 073101.

31. Watson, M. D.; Beales, A. M.; King, P. D. C., On the origin of the anomalous peak in the resistivity of $TiSe_2$. *Physical Review B* **2019,** *99* (19), 195142.
32. Walmsley, T. S.; Chamlagain, B.; Rijal, U.; Wang, T.; Zhou, Z.; Xu, Y. Q., Gate‐Tunable Photoresponse Time in Black Phosphorus‐MoS_2 Heterojunctions. *Advanced Optical Materials* **2019,** *7* (5), 1800832.
33. Wang, T.; Xu, Y.-Q., Photonic Structure-Integrated Two-Dimensional Material Optoelectronics. *Electronics* **2016,** *5* (4), 93.
34. Liu, Y.; Stradins, P.; Wei, S.-H., Van der Waals metal-semiconductor junction: Weak Fermi level pinning enables effective tuning of Schottky barrier. *Science Advances* **2016,** *2* (4), e1600069.
35. Buscema, M.; Barkelid, M.; Zwiller, V.; van der Zant, H. S. J.; Steele, G. A.; Castellanos-Gomez, A., Large and Tunable Photothermoelectric Effect in Single-Layer MoS_2. *Nano Letters* **2013,** *13* (2), 358-363.
36. Hong, T.; Chamlagain, B.; Hu, S.; Weiss, S. M.; Zhou, Z.; Xu, Y.-Q., Plasmonic Hot Electron Induced Photocurrent Response at MoS_2–Metal Junctions. *ACS Nano* **2015,** *9* (5), 5357-5363.
37. Nayeb Sadeghi, S.; Zebarjadi, M.; Esfarjani, K., Non-linear enhancement of thermoelectric performance of a $TiSe_2$ monolayer due to tensile strain, from first-principles calculations. *Journal of Materials Chemistry C* **2019,** *7* (24), 7308-7317.
38. Lakhani, A. A.; Jandl, S.; Ayache, C.; Jay-Gerin, J. P., Thermoelectric power of $TiSe_{2-x}S_x$. *Physical Review B* **1983,** *28* (4), 1978-1982.
39. Lopez-Castillo, J. M.; Amara, A.; Jandl, S.; Jay-Gerin, J. P.; Ayache, C.; Aubin, M. J., Phonon-drag effect in $TiSe_{2-x}S_x$ mixed compounds. *Physical Review B* **1987,** *36* (8), 4249-4253.
40. McIver, J. W.; Hsieh, D.; Steinberg, H.; Jarillo-Herrero, P.; Gedik, N., Control over topological insulator photocurrents with light polarization. *Nature Nanotechnology* **2012,** *7* (2), 96-100.
41. Wang, T.; Andrews, K.; Bowman, A.; Hong, T.; Koehler, M.; Yan, J.; Mandrus, D.; Zhou, Z.; Xu, Y.-Q., High-Performance WSe_2 Phototransistors with 2D/2D Ohmic Contacts. *Nano Letters* **2018,** *18*, 2766-2771.
42. Ornelas, C. D.; Bowman, A.; Walmsley, T. S.; Wang, T.; Andrews, K.; Zhou, Z.; Xu, Y.-Q., Ultrafast Photocurrent Response and High Detectivity in Two-Dimensional $MoSe_2$-based Heterojunctions. *ACS Applied Materials & Interfaces* **2020,** *12* (41), 46476-46482.
43. Li, G.; Hu, W. Z.; Qian, D.; Hsieh, D.; Hasan, M. Z.; Morosan, E.; Cava, R. J.; Wang, N. L., Semimetal-to-Semimetal Charge Density Wave Transition in $TiSe_2$. *Physical Review Letters* **2007,** *99* (2), 027404.
44. Bass, M., *Handbook of Optics: Devices, Measurements, and Properties*. McGraw-Hill Professoinal: 1994; p 1568.
45. Wang, L.; Liu, C.; Chen, X.; Zhou, J.; Hu, W.; Wang, X.; Li, J.; Tang, W.; Yu, A.; Wang, S.-W.; Lu, W., Toward Sensitive Room-Temperature Broadband Detection from Infrared to Terahertz with Antenna-Integrated Black Phosphorus Photoconductor. *Advanced Functional Materials* **2017,** *27* (7), 1604414.
46. Wu, J.; Zhao, Y.; Sun, M.; Zheng, M.; Zhang, G.; Liu, X.; Chi, D., Enhanced photoresponse of highly air-stable palladium diselenide by thickness engineering. *Nanophotonics* **2020,** *9* (8), 2467-2474.

47. Wei, R.; Tian, X.; Yang, L.; Yang, D.; Ma, Z.; Guo, H.; Qiu, J., Ultrafast and large optical nonlinearity of a TiSe2 saturable absorber in the 2 μm wavelength region. *Nanoscale* **2019,** *11* (46), 22277-22285.
48. Velebit, K.; Popčević, P.; Batistić, I.; Eichler, M.; Berger, H.; Forró, L.; Dressel, M.; Barišić, N.; Tutiš, E., Scattering-dominated high-temperature phase of 1T-$TiSe_2$: An optical conductivity study. *Physical Review B* **2016,** *94* (7), 075105.
49. Wang, T.; Zhu, Y.; Mao, Z.; Xu, Y.-Q., Tunneling Effects in Crossed $Ta_2Pt_3Se_8$–$Ta_2Pd_3Se_8$ Nanowire Junctions: Implications for Anisotropic Photodetectors. *ACS Applied Nano Materials* **2021,** *4* (2), 1817-1824.
50. Walmsley, T. S.; Andrews, K.; Wang, T.; Haglund, A.; Rijal, U.; Bowman, A.; Mandrus, D.; Zhou, Z.; Xu, Y.-Q., Near-infrared optical transitions in PdSe2 phototransistors. *Nanoscale* **2019,** *11* (30), 14410-14416.